

# ASSNet: Adaptive Semantic Segmentation Network for Microtumors and Multi-Organ Segmentation

Fuchen Zheng<sup>12</sup>, Xinyi Chen<sup>3</sup>, Xuhang Chen<sup>12</sup>, Haolun Li<sup>1</sup>, Xiaojiao Guo<sup>1</sup>, Guoheng Huang<sup>4</sup>,  
Chi-Man Pun<sup>1\*</sup>, and Shoujun Zhou<sup>2\*</sup>

<sup>1</sup>University of Macau

<sup>2</sup>Shenzhen Institute of Advanced Technology, Chinese Academy of Sciences

<sup>3</sup>Southern University of Science and Technology

<sup>4</sup>Guangdong University of Technology

**Abstract**—Medical image segmentation, a crucial task in computer vision, facilitates the automated delineation of anatomical structures and pathologies, supporting clinicians in diagnosis, treatment planning, and disease monitoring. Recent advancements in deep learning, particularly convolutional neural networks (CNNs) with U-shaped architectures, vision transformers, and Segment Anything Models (SAM), have significantly enhanced segmentation accuracy. Notably, transformers employing shifted window-based self-attention have demonstrated exceptional performance. However, their reliance on local window attention limits the fusion of local and global contextual information, crucial for segmenting microtumors and miniature organs. To address this limitation, we propose the Adaptive Semantic Segmentation Network (ASSNet), a transformer architecture that effectively integrates local and global features for precise medical image segmentation. ASSNet comprises a transformer-based U-shaped encoder-decoder network. The encoder utilizes shifted window self-attention across five resolutions to extract multi-scale features, which are then propagated to the decoder through skip connections. We introduce an augmented multi-layer perceptron within the encoder to explicitly model long-range dependencies during feature extraction. Recognizing the constraints of conventional symmetrical encoder-decoder designs, we propose an Adaptive Feature Fusion (AFF) decoder to complement our encoder. This decoder incorporates three key components: the Long Range Dependencies (LRD) block, the Multi-Scale Feature Fusion (MFF) block, and the Adaptive Semantic Center (ASC) block. These components synergistically facilitate the effective fusion of multi-scale features extracted by the decoder while capturing long-range dependencies and refining object boundaries. Comprehensive experiments on diverse medical image segmentation tasks, including multi-organ, liver tumor, and bladder tumor segmentation, demonstrate that ASSNet achieves state-of-the-art results. Code and models are available at: <https://github.com/Izeeorno/ASSNet>.

**Index Terms**—Medical Image Segmentation, Tumor Segmentation, Vision Transformer, Attention Mechanism, Multi-scale Feature Fusion, Long-Range Dependencies

## I. INTRODUCTION

By accurately delineating anatomical structures, segmentation enhances the clarity of medical images, significantly improving diagnostic accuracy and efficiency for healthcare professionals. Current research in medical image segmentation focuses on critical tasks such as tumor segmentation and organ

delineation. Consequently, neural network architectures from the broader field of computer vision are being increasingly adapted for medical image analysis. Vision transformers [1], exemplified by the Swin-transformer [2], have gained significant traction due to their robust feature extraction capabilities. However, while advancements in window attention mechanisms within these transformers have yielded impressive results, challenges remain. These models often struggle to capture features of small objects due to limitations in modeling long-range dependencies [3] and accurately delineating image edges. Consequently, effectively integrating multi-scale local and global features remains an ongoing challenge.

To address these limitations, we propose the Adaptive Semantic Segmentation Network (ASSNet), a novel Transformer-based [4] architecture specifically designed for medical image segmentation. Inspired by the strengths of ResUnet [5] and Swin-transformer [2], ASSNet leverages Transformer blocks within a U-shaped residual structure to enhance feature learning across multiple scales.

Furthermore, recognizing the limitations of simply replicating encoder structures in the decoder, we introduce a novel Adaptive Feature Fusion (AFF) decoder. This decoder comprises three key components: the Long Range Dependencies (LRD) block, the Multi-Scale Feature Fusion (MFF) block, and the Adaptive Semantic Center (ASC) block. These components work synergistically to leverage encoder-derived features effectively, enabling the accurate segmentation of small structures, particularly at edges, and facilitating robust multi-scale feature fusion.

Our straightforward residual U-shaped Transformer architecture, without relying on complex multi-scale structures or intricate loss functions, achieves state-of-the-art performance on various medical image segmentation tasks. Notably, ASSNet surpasses previous state-of-the-art models, demonstrating impressive improvements on the LiTS2017, ISICDM2019 and Synapse datasets, respectively. The main contributions of this paper are as follows:

1. We introduce **ASSNet**, a hybrid model that combines the strengths of ResUnet and Swin-transformer, incorporating window attention, spatial attention, U-shaped architecture, and residual connections for efficient segmentation.

\* Corresponding authors.

2. We propose an **Adaptive Feature Fusion (AFF) Decoder** that maximizes the synergistic potential of window attention to capture multi-scale local and global information by fusing feature maps of varying scales.

3. Extensive experiments demonstrate that the proposed ASSNet achieves new state-of-the-art results on various medical image segmentation datasets.

## II. RELATED WORK

### A. Medical Image Segmentation

Medical image segmentation is a fundamental task that involves partitioning medical images into distinct regions representing different anatomical structures or tissues. The U-Net architecture [6], with its elegant encoder-decoder structure and skip connections, has emerged as a leading approach for this task. Its ability to capture both fine-grained details and global context has led to widespread adoption and numerous extensions. For instance, ResUNet [7] combines the strengths of U-Net [6] and ResNet [5], leveraging the power of residual connections [8] to facilitate the training of deeper networks and mitigate the vanishing gradient problem [9]. These residual connections allow for unimpeded information flow across layers, significantly enhancing the network's ability to learn complex representations and improve segmentation accuracy.

The success of ResUNet can be attributed to the synergistic combination of residual and skip connections. While residual connections ensure efficient information propagation across layers, skip connections enable the fusion of features from corresponding levels in the encoder and decoder pathways. This fusion of multi-scale features is crucial for capturing both local details and global context, leading to improved segmentation performance. UNet++ [10] further refines the U-Net architecture by introducing dense skip connections and a nested architecture. These connections enhance information flow between encoder and decoder layers, facilitating the capture of multi-scale features and improving segmentation accuracy. Building upon these foundational concepts, ASSNet also incorporates skip connections and residual connections to optimize its segmentation capabilities.

### B. Vision Transformer and Hybrid Architectures

Unlike Convolutional Neural Networks (CNNs) that process images locally, Vision Transformer (ViT) models [1] leverage a self-attention mechanism to capture long-range dependencies within images. This global receptive field has enabled ViT to achieve state-of-the-art performance in image classification tasks. The success of ViT has inspired its adaptation to medical image analysis, with Swin Transformer [11] demonstrating impressive results in various medical imaging applications. The Swin Transformer employs a hierarchical approach, computing self-attention within local windows and then shifting these windows to capture relationships across different image regions. This strategy reduces computational complexity while preserving the ability to model long-range dependencies.

Recognizing the complementary strengths of CNNs and transformers, researchers have explored hybrid architectures

that combine these paradigms. ResT [12], [13] exemplifies this trend, integrating ResNet and transformer modules to leverage the feature extraction capabilities of both. In the realm of U-Net, the incorporation of attention mechanisms has proven beneficial. For instance, Attention U-Net [14] introduces attention gates that enable the network to focus on salient regions during segmentation. This integration of attention mechanisms has paved the way for U-shaped transformer architectures, such as TransUNet [4]. TransUNet utilizes a convolutional encoder to extract features and a transformer to model global context.

However, a common limitation in TransUNet and similar architectures like TransClaw [15] and TransAttUnet [16] is the suboptimal integration of attention mechanisms, preventing the full realization of the transformer's potential. To address this, our proposed network introduces a novel residual U-shaped transformer architecture designed for effective attention fusion. This architecture leverages the strengths of the window attention mechanism employed in Swin Transformer and enhances it with an Enhanced Forward Feedback Network (EFFN), resulting in superior performance for medical image segmentation.

## III. METHODOLOGY

This section outlines the architecture and functionality of ASSNet. We first describe the network's overall pipeline, followed by a detailed exposition of the Multi-scale Window Attention (MWA) Transformer block—the core encoder component. Subsequently, we elucidate the Adaptive Feature Fusion (AFF) decoder, which is crucial for modeling long-range dependencies and enhancing the network's ability to capture fine-grained details amidst complex edge structures.

### A. Overall Pipeline

ASSNet leverages a hierarchical U-shaped architecture, as illustrated in Figure 1, incorporating skip connections and residual connections between the encoder and decoder to facilitate efficient information propagation.

The input image, of size  $C \times H \times W$  (where  $C$ ,  $H$ , and  $W$  represent channels, height, and width, respectively), is processed through patch partition and linear embedding layers before entering the window attention module embedded in the MWA block. Following the original Swin Transformer [11], the encoder consists of four stages, each performing  $2 \times C$  spatial downsampling in the patch merging layer. This layer concatenates features from  $2 \times 2$  spatially neighboring patches and applies a linear projection to halve their dimension.

The decoder mirrors the encoder with four symmetrical stages, incorporating our proposed Adaptive Feature Fusion (AFF) decoder. The AFF decoder facilitates the fusion of high-level semantic information with low-level spatial details, surpassing the decoders of current state-of-the-art models [11], [17], [18]. Finally, an output convolution layer processes the concatenated features to generate the segmentation prediction.

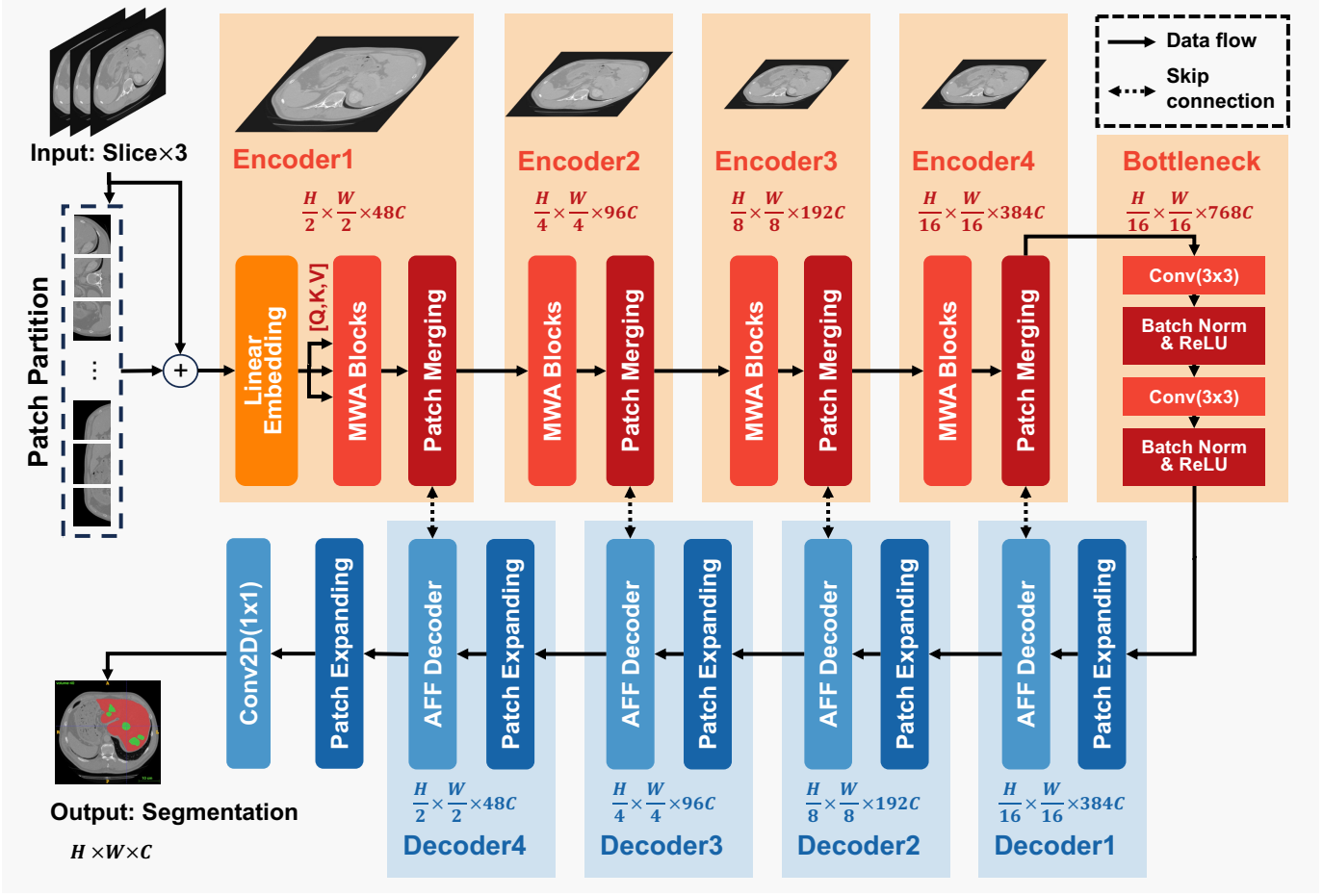


Fig. 1. Overview of the ASSNet architecture.

### B. MWA Transformer Block

The MWA Transformer block forms the backbone of ASSNet. As shown in Figure 2, it substitutes the Multi-Head Self-Attention (MSA) module [19] in the standard Transformer layer with a shifted window attention-based MSA module, while preserving other attention-related components. Each MWA block consists of a shifted window-based MSA module followed by an Enhanced Feed-Forward Network (EFFN).

Recognizing the limitations of standard FFNs in capturing local context [20], [21], we enhance the MLP within our Transformer block by incorporating depth-wise and pixel-wise convolutions [22]–[24]. As depicted in Figure 2, the EFFN first projects input tokens to a higher dimensional space. The projected tokens are then reshaped into 2D feature maps and processed by a  $3 \times 3$  pixel-wise convolution followed by a  $3 \times 3$  depth-wise convolution, effectively capturing local contextual information. Subsequently, the features are reshaped back into tokens and projected back to the original channel dimension. Finally, a GELU activation function [25] introduces non-linearity.

Mathematically, the computation within an MWA trans-

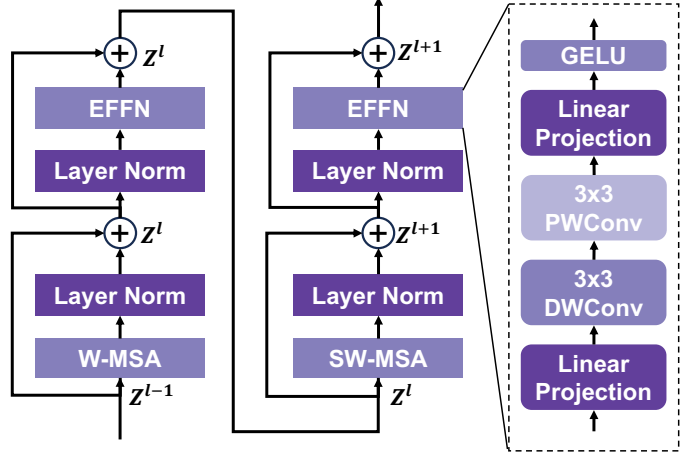


Fig. 2. This figure presents details of a schematic diagram of the proposed Multi-scale Window Attention (MWA) transformer block.

former block can be expressed as:

$$\begin{aligned}
 \hat{X}^l &= \text{W-MSA}(\text{LN}(X^{l-1})) + X^{l-1}, \\
 X^l &= \text{EFFN}(\text{LN}(\hat{X}^l)) + \hat{X}^l, \\
 \hat{X}^{l+1} &= \text{SW-MSA}(\text{LN}(X^l)) + X^l, \\
 X^{l+1} &= \text{EFFN}(\text{LN}(\hat{X}^{l+1})) + \hat{X}^{l+1},
 \end{aligned} \tag{1}$$

where  $\hat{X}^l$  and  $\hat{X}^{l+1}$  represent the output from window-based multi-head self-attention using regular (W-MSA) and shifted window partitioning configurations (SW-MSA), respectively; LN and EFFN denote layer normalization and the proposed enhanced feed-forward network illustrated in Figure 2, respectively.

Following previous work [18], [26], we incorporate a relative position bias  $B$  within the self-attention computation to enhance performance. The attention calculation is formulated as:

$$\text{Attention}(Q, K, V) = \text{SoftMax} \left( \frac{QK^T}{\sqrt{d}} + B \right) V, \quad (2)$$

where  $B$  is derived from a smaller parameterized bias matrix  $\hat{B} \in \mathbb{R}^{(2M-1) \times (2M-1)}$ ;  $Q$ ,  $K$ , and  $V$  represent the query, key, and value matrices, respectively; and  $d$  is the dimension of the query and key features.

The synergistic interplay between W-MSA, SW-MSA, and EFFN within each Transformer block enables ASSNet to effectively capture both global and local contextual information, leading to improved segmentation performance.

### C. Adaptive Feature Fusion (AFF) Decoder

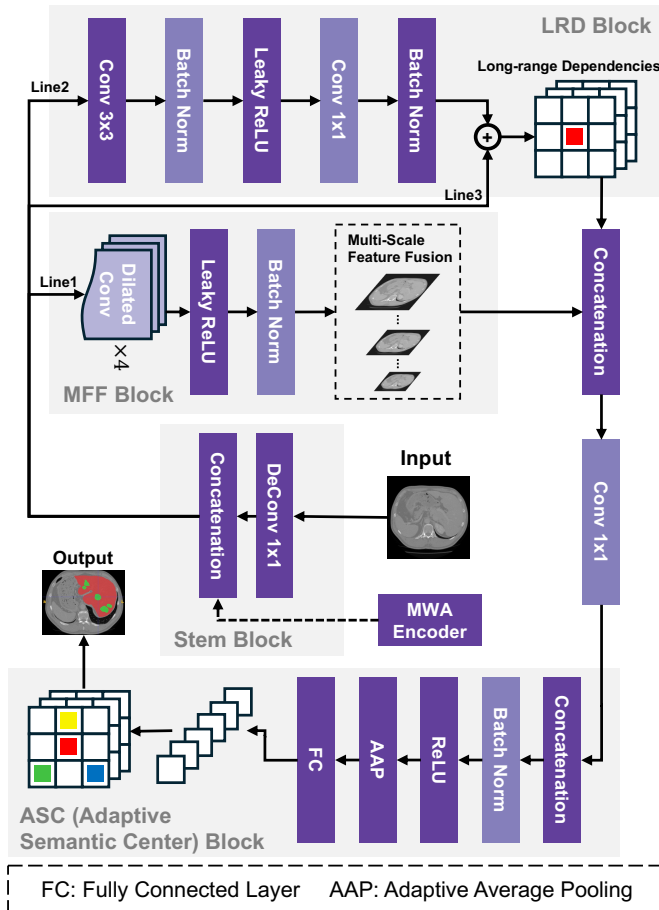


Fig. 3. This figure presents details of a schematic diagram of the proposed Adaptive Feature Fusion (AFF) Decoder.

To address the limitations of vision transformers in capturing local dependencies [3], [26] and the inadequacies of existing decoders in integrating multi-scale local and global features [11], [17], [18], we propose an Adaptive Feature Fusion (AFF) Decoder. The AFF decoder comprises Long-Range Dependencies (LRD) block, Multi-scale Feature Fusion (MFF) block, and Adaptive Semantic Center (ASC) block, as illustrated in Figure 3.

The AFF decoder begins with a standard deconvolution operation to restore the feature map to the original image size while preserving resolution. Subsequently, skip connections are employed to concatenate MWA encoder feature maps from different scales, enriching the feature map with multi-scale information. This enriched feature map then undergoes three parallel operations. First, spatial attention using dilated convolutions with dilation rates of 1, 6, 12, and 18 is applied to capture multi-scale details [27]. LeakyReLU [28] is utilized as the activation function in the decoder to mitigate the vanishing gradient problem and enhance model stability and generalization. Second, an LRD block, implemented using a series of convolutions and LeakyReLU activations, models long-range dependencies. Finally, inspired by ResNet [5], a third parallel thread acts as a mask prompt, aiding the decoding process of the first two threads. The outputs from these three threads are then concatenated and processed by a convolution operation.

The resulting feature map is then passed to the ASC block. Drawing inspiration from the Sobel edge detection method [29], the ASC block extracts local region information and performs channel-wise enhancement. It achieves this by utilizing an enhanced filter generated from adaptive average pooling [30] and a fully connected layer [31].

### D. Objective Function

During training, ASSNet employs the BCE Dice loss  $\mathcal{L}_{BD}$  [32], a combination of Binary Cross-Entropy (BCE) loss  $\mathcal{L}_{BCE}$  and Dice loss  $\mathcal{L}_D$ , widely used in medical image segmentation tasks. This loss function is defined as:

$$\begin{aligned} \mathcal{L}_{BD} = & \mathcal{L}_D + \mathcal{L}_{BCE}(y, p) \\ = & \frac{1}{N} \sum_{i=1}^N \left( 1 - \frac{2 \sum_j y_{i,j} p_{i,j}}{\sum_j y_{i,j} + \sum_j p_{i,j}} \right) \\ & - (y \log(p) + (1 - y) \log(1 - p)), \end{aligned} \quad (3)$$

where  $y$  represents the ground truth segmentation mask,  $p$  denotes the predicted segmentation mask, and  $N$  is the number of pixels in the image. BCE loss penalizes discrepancies between the predicted and actual label distributions, while Dice loss encourages overlap between the predicted and actual segmentation regions. This combination effectively enhances both pixel-wise classification accuracy and boundary delineation.

## IV. EXPERIMENTS

In this section, we present the experimental framework and discuss the results. First, we describe the datasets and

evaluation metrics employed. Next, we compare the performance of ASSNet against state-of-the-art methods in medical image segmentation. Finally, we conduct ablation studies to investigate the impact of individual components in the ASSNet architecture.

#### A. Datasets and Implementation Details

To ensure a comprehensive evaluation and fair comparison with existing methods, we conducted experiments on three public medical image datasets:

- 1) **LiTS2017** [37]: This dataset focuses on liver tumor segmentation and comprises 131 contrast-enhanced 3D abdominal CT scans.
- 2) **ISICDM2019** [38]: This dataset centers on bladder tumor segmentation and includes 2200 bladder cancer images.
- 3) **Synapse** [39]: This dataset targets multi-organ segmentation and consists of 40 3D abdominal CT scans with multiple organs.

In all experiments, we adhered to the training, validation, and test splits provided by nnformer [34] to ensure consistency and facilitate fair comparisons with other methods. This resulted in splits of 80%, 15%, and 5% for training, validation, and testing, respectively. All input images were resized to a resolution of  $512 \times 512$  pixels.

We implemented ASSNet using the PyTorch framework and trained the model on a single NVIDIA GeForce RTX 4090 GPU. The Stochastic Gradient Descent (SGD) [40] optimizer was employed with a momentum of 0.98 and a weight decay of  $1 \times 10^{-6}$ . The initial learning rate was set to  $1 \times 10^{-2}$  and was subsequently decreased using a cosine decay strategy to a minimum of  $6 \times 10^{-6}$ . Data augmentation during training included random horizontal flipping and rotation. The reported results represent the mean of five-fold cross-validation. Some comparison results are referenced from nnformer [34], TransUNet [4], SAM [41], [42], and MedSAM2 [43].

#### B. Evaluation Metrics

We assessed the segmentation performance using two widely recognized metrics:

1) *Dice Coefficient Score* [46]: The Dice Similarity Coefficient (DSC) quantifies the overlap between the predicted segmentation and the ground truth. Its value ranges from 0 to 1, with higher values indicating superior segmentation performance.

$$DSC = \frac{2 \times |P \cap G|}{|P| + |G|}, \quad (4)$$

In this context,  $P$  denotes the predicted segmentation, while  $G$  represents the ground truth segmentation. The term  $|P \cap G|$  indicates the number of pixels in the intersection of the predicted and ground truth segmentations, whereas  $|P|$  and  $|G|$  denote the number of pixels in the predicted and ground truth segmentations, respectively.

2) *Mean Intersection over Union (mIoU)*: The mean Intersection over Union (mIoU) calculates the average ratio of intersection to union between the predicted segmentation and the ground truth across all classes. It is defined as:

$$mIoU = \frac{1}{C} \sum_{i=1}^C \frac{|P_i \cap G_i|}{|P_i| + |G_i| - |P_i \cap G_i|}, \quad (5)$$

where  $C$  is the number of classes,  $P_i$  represents the predicted segmentation for class  $i$ , and  $G_i$  represents the ground truth segmentation for class  $i$ . Similar to DSC, mIoU ranges from 0 to 1, with higher values indicating better segmentation performance.

#### C. Comparisons with State-of-the-Art Methods

We compared the performance of ASSNet with several state-of-the-art medical image segmentation methods on the three datasets described above. The results are summarized in Tables I and II.

1) *Liver Tumor Segmentation*: Table I presents the results on the LiTS2017 dataset. ASSNet outperforms all other methods, achieving an average DSC of 95.47% and an mIoU of 94.88%. Notably, ASSNet surpasses the second-best model, TransUNet [4], by a significant margin (DSC: +2.19%, mIoU: +4.07%). This improvement highlights ASSNet's ability to accurately segment small and irregularly shaped tumors, which can be attributed to the Multi-Scale Feature Fusion (MFF) block within the AFF Decoder. The MFF block effectively captures features across multiple scales, enabling the network to delineate fine-grained tumor boundaries. Furthermore, the Adaptive Spatial Feature Fusion (ASFF) block and Long-Range Dependency (LRD) block further enhance ASSNet's ability to preserve essential information and capture long-range spatial dependencies, crucial for accurate segmentation. Interestingly, even when trained on large medical datasets, the popular segmentation models SAM [35], [41] and MedSAM [36] struggle to accurately segment multiple tumors with varying shapes and sizes within a single image. This suggests that ASSNet's architectural advantages provide it with an edge in handling such complex segmentation scenarios.

2) *Bladder Tumor Segmentation*: On the ISICDM2019 dataset, ASSNet again demonstrates superior performance, achieving an average DSC of 96.75% and an mIoU of 96.04% as shown in Table I. This represents a substantial improvement of 3.25% in DSC compared to the second-best method. The remarkable performance on bladder tumor segmentation can be attributed to the ASC block in the AFF decoder, which effectively captures local region information critical for accurate boundary delineation. These results underscore the robustness and adaptability of ASSNet across different tumor types and imaging modalities.

3) *Multi-Organ Segmentation*: The results for the Synapse multi-organ segmentation dataset are presented in Table II. While ASSNet achieves state-of-the-art results with an average DSC of 90.73%, it slightly trails the best-performing method on three out of eight metrics. However, it is important to note that ASSNet consistently achieves high scores across

TABLE I  
COMPARISON WITH STATE-OF-THE-ART MODELS ON THE ISICDM2019 AND LITS2017 DATASETS. THE BEST RESULTS ARE BOLDED WHILE THE SECOND BEST ARE UNDERLINED.

Method	ISICDM2019				LITS2017			
	Average		Bladder	Tumor	Average		Liver	Tumor
	DSC(%) $\uparrow$	mIoU(%) $\uparrow$	DSC(%) $\uparrow$	DSC(%) $\uparrow$	DSC(%) $\uparrow$	mIoU(%) $\uparrow$	DSC(%) $\uparrow$	DSC(%) $\uparrow$
R50-ViT [1]+CUP [4]	88.77	85.62	92.05	85.49	82.62	79.68	85.83	79.41
TransUNet [4]	<u>94.56</u>	<u>93.60</u>	<u>97.74</u>	<u>91.38</u>	<u>93.29</u>	<u>90.81</u>	<u>95.54</u>	<u>91.03</u>
SwinUNet [17]	91.95	89.77	94.73	89.17	89.68	86.62	93.31	86.04
Swin UNETR [18]	92.60	90.61	95.08	90.12	91.95	90.02	94.73	89.17
UNETR [33]	91.55	88.34	94.83	88.26	89.38	87.46	92.89	85.86
nnFormer [34]	93.69	89.11	96.97	90.41	91.74	89.95	94.57	88.91
SAM [35]+Manual Prompt	34.16	23.4	59.10	9.22	27.33	17.21	46.10	8.56
MedSAM [36]	53.17	37.16	65.3	41.03	73.36	60.73	90.1	56.61
<b>ASSNet (Ours)</b>	<b>96.75</b>	<b>96.04</b>	<b>98.87</b>	<b>94.63</b>	<b>95.47</b>	<b>94.88</b>	<b>96.79</b>	<b>94.14</b>

TABLE II  
COMPARISON WITH STATE-OF-THE-ART MODELS ON THE SYNAPSE MULTI-ORGAN DATASET. THE BEST RESULTS ARE BOLDED WHILE THE SECOND BEST ARE UNDERLINED.

Model	Average DSC(%) $\uparrow$	Aotra DSC(%) $\uparrow$	Gallbladder DSC(%) $\uparrow$	Kidney(Left) DSC(%) $\uparrow$	Kidney(Right) DSC(%) $\uparrow$	Liver DSC(%) $\uparrow$	Pancreas DSC(%) $\uparrow$	Spleen DSC(%) $\uparrow$	Stomach DSC(%) $\uparrow$
R50-ViT [1]+CUP [4]	71.29	73.73	55.13	75.80	72.20	91.51	45.99	81.99	73.95
TransUNet [4]	84.37	<u>90.68</u>	71.99	86.04	83.71	<u>95.54</u>	73.96	88.80	84.20
SwinUNet [17]	79.13	85.47	66.53	83.28	79.61	94.29	56.58	90.66	76.60
UNETR [33]	79.57	89.99	60.56	85.66	84.80	94.46	59.25	87.81	73.99
Swin UNETR [18]	83.51	<u>90.75</u>	66.72	86.51	85.88	95.33	70.07	<b>94.59</b>	78.20
CoTr [44]	80.74	85.42	68.93	85.45	83.62	93.89	63.77	88.58	76.23
nnFormer [34]	85.32	90.72	71.67	85.60	87.02	<u>96.28</u>	82.28	87.30	81.69
SAM [35]+Manual Prompt	58.55	61.20	54.30	79.10	68.60	46.10	51.10	51.80	56.20
MedSAM [36]	82.55	87.20	76.60	88.50	81.40	90.10	76.00	75.10	85.50
SAM 2 [45]	53.39	40.00	77.20	64.20	72.40	27.00	68.20	36.60	41.50
MedSAM-2 [43]	<u>89.08</u>	89.40	<b>92.70</b>	<u>92.10</u>	<u>92.40</u>	83.60	<b>83.20</b>	91.80	<u>87.40</u>
<b>ASSNet (Ours)</b>	<b>90.73</b>	<b>93.02</b>	<u>87.08</u>	<b>92.67</b>	<b>93.06</b>	<b>97.11</b>	<u>82.97</u>	<u>92.19</u>	<b>87.72</b>

all organs, demonstrating its ability to generalize to different anatomical structures. Notably, ASSNet excels in segmenting smaller organs, achieving the highest DSC scores for five out of the eight organs. This robust performance on a challenging multi-organ dataset highlights the effectiveness of ASSNet’s U-shaped architecture and AFF decoder in preserving both high-level semantic information and low-level spatial details, which are crucial for accurate multi-organ segmentation.

#### D. Visualization of Segmentation Results

To visually assess the segmentation capabilities of ASSNet, Figure 4 presents qualitative comparisons against other state-of-the-art methods on representative slices from the LiTS2017, ISICDM2019, and Synapse datasets. ASSNet consistently demonstrates superior performance in delineating both organ and tumor boundaries compared to the other models. In particular, ASSNet accurately segments small tumor nodules on the liver periphery and preserves the integrity of miniature organs, which are often missed or inaccurately segmented by other methods. These visual comparisons further emphasize the accuracy and robustness of ASSNet in challenging medical image segmentation scenarios.

#### E. Ablation Study

To investigate the contribution of each module within ASSNet, we conducted an ablation study on the ISICDM2019 and LiTS2017 datasets. We used the same experimental setup as described in Section IV-A and evaluated the performance of ASSNet by removing one component at a time. The results, summarized in Table III, demonstrate that all components contribute to the overall performance of ASSNet.

TABLE III  
ABLATION STUDY OF DIFFERENT MODULES IN ASSNET.

EFFN	LRD	MFF	ASC	ISICDM2019 Average DSC $\uparrow$	LiTS2017 Average DSC $\uparrow$
$\times$	✓	✓	✓	93.91%	92.56%
✓	$\times$	✓	✓	75.54%	73.92%
✓	✓	$\times$	✓	87.15%	85.10%
✓	✓	✓	$\times$	88.93%	87.22%
✓	✓	✓	✓	96.75%	95.47%

The ablation study clearly shows that the Embedded Feature Fusion Network (EFFN) significantly enhances ASSNet’s abil-

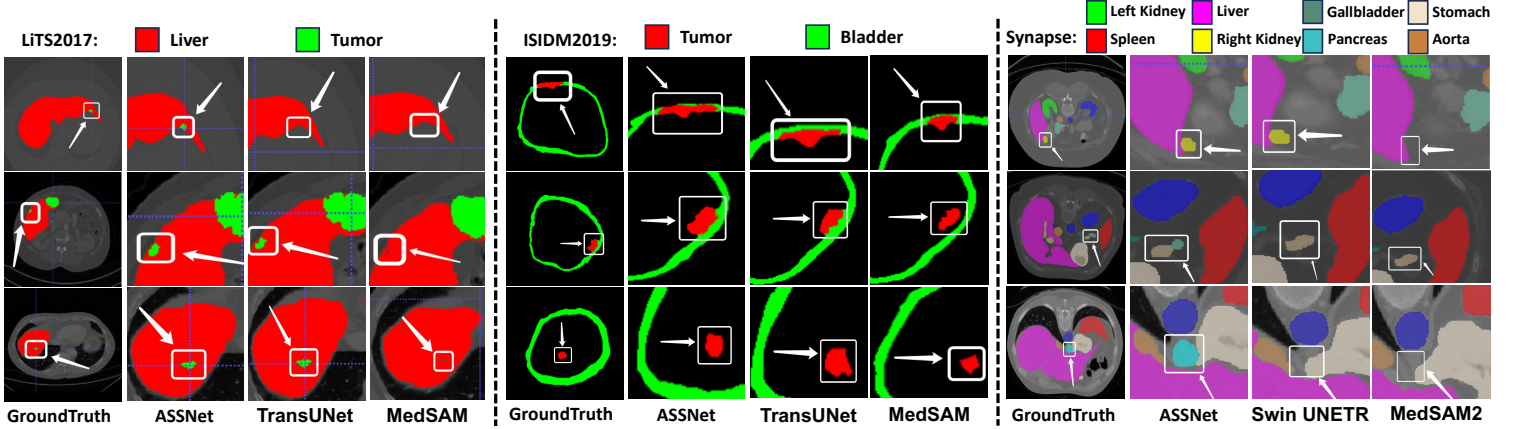


Fig. 4. LiTS2017, ISICDM2019 and Synapse Prediction Results

ity to model long-range dependencies. Removing EFFN leads to a considerable drop in performance, with the average DSC decreasing to 93.91% and 92.56% for the ISICDM2019 and LiTS2017 datasets, respectively. This highlights the importance of EFFN in capturing long-range interactions between image regions, which are essential for accurate segmentation.

Similarly, the LRD block in the AFF decoder plays a crucial role in preserving long-range dependencies and establishing a connection between the encoder and decoder. Removing the LRD block results in a substantial decline in performance, with average DSCs dropping to 75.54% and 73.92% for the two datasets, respectively. This confirms the essential function of the LRD block in bridging the gap between the encoder and decoder, enabling the network to effectively leverage information from both low-level and high-level features.

The MFF and ASC blocks within the decoder also contribute significantly to ASSNet’s state-of-the-art performance. The MFF block enables ASSNet to fuse features across multiple scales, which is crucial for accurately segmenting structures of varying sizes. Removing the MFF block leads to a decrease in average DSC to 87.15% and 85.10% for the two datasets, respectively, demonstrating the importance of multi-scale feature fusion in medical image segmentation. The ASC block, on the other hand, focuses on detecting critical edges and central features, which are essential for accurate boundary delineation. Removing the ASC module results in a reduction in average DSC to 88.93% and 87.22%, respectively, highlighting its importance in capturing fine-grained details and ensuring the integrity of segmented structures.

In summary, the ablation study confirms the efficacy of each component in ASSNet and provides valuable insights for future model enhancements. The results emphasize the importance of long-range dependency modeling, multi-scale feature fusion, and edge detection in achieving high-performance medical image segmentation.

## V. CONCLUSION

This paper presented ASSNet, a novel Transformer-based architecture purpose-built for accurate and efficient medical

image segmentation. The hallmark of ASSNet lies in its innovative MWA encoder and AFF decoder. By effectively integrating an efficient feedforward network block, a long-range dependency block, a multi-scale feature fusion block, and an adaptive spatial-channel attention block, ASSNet exhibits superior capacity in modeling long-range dependencies and capturing salient features across varying scales and spatial contexts. Rigorous evaluation on three publicly available medical image segmentation datasets demonstrated that ASSNet consistently achieves state-of-the-art segmentation performance, surpassing existing methods in accurately delineating diverse anatomical structures and pathologies. These promising results highlight ASSNet’s potential as a robust and valuable tool for assisting medical professionals in critical tasks such as diagnosis, treatment planning, and disease monitoring. Future research will investigate the generalizability of ASSNet to other medical imaging modalities and further evaluate its performance in more complex clinical scenarios.

## ACKNOWLEDGMENT

This work was supported in part by the National Key R&D Project of China (2018YFA0704102, 2018YFA0704104), in part by Natural Science Foundation of Guangdong Province (No. 2023A1515010673), and in part by Shenzhen Technology Innovation Commission (No. JSGG2022083111040001), in part by Shenzhen Development and Reform Commission (No. XMHT20220104009).

## REFERENCES

- [1] A. Dosovitskiy, L. Beyer, A. Kolesnikov, D. Weissenborn, X. Zhai, T. Unterthiner, M. Dehghani, M. Minderer, G. Heigold, S. Gelly, J. Uszkoreit, and N. Houlsby, “An image is worth 16x16 words: Transformers for image recognition at scale,” in *International Conference on Learning Representations*, 2021. [1](#), [2](#), [6](#)
- [2] Z. Liu, Y. Lin, Y. Cao, H. Hu, Y. Wei, Z. Zhang, S. Lin, and B. Guo, “Swin transformer: Hierarchical vision transformer using shifted windows,” in *Proceedings of the IEEE/CVF international conference on computer vision*, 2021, pp. 9992–10 002. [1](#)
- [3] S. Wang, L. Zhou, Z. Gan, Y.-C. Chen, Y. Fang, S. Sun, Y. Cheng, and J. Liu, “Cluster-former: Clustering-based sparse transformer for long-range dependency encoding,” *arXiv*, 2020. [1](#), [4](#)

[4] J. Chen, Y. Lu, Q. Yu, X. Luo, E. Adeli, Y. Wang, L. Lu, A. L. Yuille, and Y. Zhou, "Transunet: Transformers make strong encoders for medical image segmentation," *ArXiv*, 2021. [1](#), [2](#), [5](#), [6](#)

[5] K. He, X. Zhang, S. Ren, and J. Sun, "Deep residual learning for image recognition," in *Proceedings of the IEEE/CVF conference on computer vision and pattern recognition*, 2016, pp. 770–778. [1](#), [2](#), [4](#)

[6] O. Ronneberger, P. Fischer, and T. Brox, "U-net: Convolutional networks for biomedical image segmentation," in *Medical image computing and computer-assisted intervention*, 2015, pp. 234–241. [2](#)

[7] F. I. Diakogiannis, F. Waldner, P. Caccetta, and C. Wu, "Resunet-a: A deep learning framework for semantic segmentation of remotely sensed data," *ISPRS Journal of Photogrammetry and Remote Sensing*, vol. 162, pp. 94–114, 2020. [2](#)

[8] C. Szegedy, S. Ioffe, V. Vanhoucke, and A. A. Alemi, "Inception-v4, inception-resnet and the impact of residual connections on learning," in *Proceedings of the AAAI conference on artificial intelligence*, 2017, pp. 4278–4284. [2](#)

[9] K. Zhang, W. Zuo, Y. Chen, D. Meng, and L. Zhang, "Beyond a gaussian denoiser: Residual learning of deep cnn for image denoising," *IEEE Transactions on Image Processing*, vol. 26, no. 7, pp. 3142–3155, 2017. [2](#)

[10] Z. Zhou, M. M. R. Siddiquee, N. Tajbakhsh, and J. Liang, "Unet++: Redesigning skip connections to exploit multiscale features in image segmentation," *IEEE Transactions on Medical Imaging*, 2019. [2](#)

[11] Z. Liu, Y. Lin, Y. Cao, H. Hu, Y. Wei, Z. Zhang, S. Lin, and B. Guo, "Swin transformer: Hierarchical vision transformer using shifted windows," in *Proceedings of the IEEE/CVF international conference on computer vision*, 2021, pp. 9992–10002. [2](#), [4](#)

[12] Q. Zhang and Y. Yang, "Rest: An efficient transformer for visual recognition," in *Advances in Neural Information Processing Systems*, 2021, pp. 15475–15485. [2](#)

[13] Q. Zhang and Y.-B. Yang, "Rest v2: simpler, faster and stronger," *Advances in Neural Information Processing Systems*, vol. 35, pp. 36440–36452, 2022. [2](#)

[14] O. Oktay, J. Schlemper, L. L. Folgoc, M. Lee, M. Heinrich, K. Misawa, K. Mori, S. McDonagh, N. Y. Hammerla, B. Kainz *et al.*, "Attention u-net: Learning where to look for the pancreas," *ArXiv*, 2018. [2](#)

[15] Y. Chang, H. Menghan, Z. Guangtao, and Z. Xiao-Ping, "Transclaw u-net: Claw u-net with transformers for medical image segmentation," *ArXiv*, 2021. [2](#)

[16] B. Chen, Y. Liu, Z. Zhang, G. Lu, and A. W. K. Kong, "Transattunet: Multi-level attention-guided u-net with transformer for medical image segmentation," *IEEE Transactions on Emerging Topics in Computational Intelligence*, 2023. [2](#)

[17] H. Cao, Y. Wang, J. Chen, D. Jiang, X. Zhang, Q. Tian, and M. Wang, "Swin-unet: Unet-like pure transformer for medical image segmentation," in *ECCV*, 2022, pp. 205–218. [2](#), [4](#), [6](#)

[18] Y. Tang, D. Yang, W. Li, H. R. Roth, B. Landman, D. Xu, V. Nath, and A. Hatamizadeh, "Self-supervised pre-training of swin transformers for 3d medical image analysis," in *Proceedings of the IEEE/CVF conference on computer vision and pattern recognition*, 2022, pp. 20730–20740. [2](#), [4](#), [6](#)

[19] A. Vaswani, N. Shazeer, N. Parmar, J. Uszkoreit, L. Jones, A. N. Gomez, L. Kaiser, and I. Polosukhin, "Attention is all you need," in *Advances in Neural Information Processing Systems*, 2017, pp. 5998–6008. [3](#)

[20] H. Wu, B. Xiao, N. Codella, M. Liu, X. Dai, L. Yuan, and L. Zhang, "Cvt: Introducing convolutions to vision transformers," in *Proceedings of the IEEE/CVF international conference on computer vision*, 2021, pp. 22–31. [3](#)

[21] T. Huang, S. Li, X. Jia, H. Lu, and J. Liu, "Neighbor2neighbor: Self-supervised denoising from single noisy images," in *Proceedings of the IEEE/CVF conference on computer vision and pattern recognition*, 2021, pp. 14781–14790. [3](#)

[22] Y. Li, K. Zhang, J. Cao, R. Timofte, and L. Van Gool, "Localvit: Bringing locality to vision transformers," *arXiv*, 2021. [3](#)

[23] M. Sandler, A. Howard, M. Zhu, A. Zhmoginov, and L.-C. Chen, "Mobilenetv2: Inverted residuals and linear bottlenecks," in *Proceedings of the IEEE/CVF conference on computer vision and pattern recognition*, 2018, pp. 4510–4520. [3](#)

[24] K. Yuan, S. Guo, Z. Liu, A. Zhou, F. Yu, and W. Wu, "Incorporating convolution designs into visual transformers," in *Proceedings of the IEEE/CVF international conference on computer vision*, 2021, pp. 579–588. [3](#)

[25] D. Hendrycks and K. Gimpel, "Gaussian error linear units (gelus)," *arXiv*, 2016. [3](#)

[26] Z. Wang, X. Cun, J. Bao, W. Zhou, J. Liu, and H. Li, "Uformer: A general u-shaped transformer for image restoration," in *Proceedings of the IEEE/CVF conference on computer vision and pattern recognition*, 2022, pp. 17683–17693. [4](#)

[27] D. Jha, P. H. Smedsrød, D. Johansen, T. de Lange, H. D. Johansen, P. Halvorsen, and M. A. Riegler, "A comprehensive study on colorectal polyp segmentation with resunet++, conditional random field and test-time augmentation," *IEEE Journal of Biomedical and Health Informatics*, vol. 25, no. 6, pp. 2029–2040, 2021. [4](#)

[28] A. L. Maas, A. Y. Hannun, A. Y. Ng *et al.*, "Rectifier nonlinearities improve neural network acoustic models," in *International conference on machine learning*, vol. 30, no. 1, 2013, p. 3. [4](#)

[29] N. Kanopoulos, N. Vasanthavada, and R. L. Baker, "Design of an image edge detection filter using the sobel operator," *IEEE Journal of solid-state circuits*, vol. 23, no. 2, pp. 358–367, 1988. [4](#)

[30] D. Yu, H. Wang, P. Chen, and Z. Wei, "Mixed pooling for convolutional neural networks," in *Rough Sets and Knowledge Technology: 9th International Conference, RSKT 2014, Shanghai, China, October 24–26, 2014, Proceedings*, 9, 2014, pp. 364–375. [4](#)

[31] A. Krizhevsky, I. Sutskever, and G. E. Hinton, "Imagenet classification with deep convolutional neural networks," *Advances in Neural Information Processing Systems*, vol. 25, 2012. [4](#)

[32] F. Milletari, N. Navab, and S.-A. Ahmadi, "V-net: Fully convolutional neural networks for volumetric medical image segmentation," in *3DV*, 2016, pp. 565–571. [4](#)

[33] A. Hatamizadeh, Y. Tang, V. Nath, D. Yang, A. Myronenko, B. Landman, H. R. Roth, and D. Xu, "Unetr: Transformers for 3d medical image segmentation," in *Proceedings of the IEEE/CVF international conference on computer vision*, 2022, pp. 574–584. [6](#)

[34] H.-Y. Zhou, J. Guo, Y. Zhang, X. Han, L. Yu, L. Wang, and Y. Yu, "nnFormer: Volumetric medical image segmentation via a 3d transformer," *IEEE Transactions on Image Processing*, 2023. [5](#), [6](#)

[35] A. Kirillov, E. Mintun, N. Ravi, H. Mao, C. Rolland, L. Gustafson, T. Xiao, S. Whitehead, A. C. Berg, W.-Y. Lo *et al.*, "Segment anything," in *Proceedings of the IEEE/CVF international conference on computer vision*, 2023, pp. 4015–4026. [5](#), [6](#)

[36] J. Ma, Y. He, F. Li, L. Han, C. You, and B. Wang, "Segment anything in medical images," *Nature Communications*, vol. 15, no. 1, p. 654, 2024. [5](#), [6](#)

[37] P. Bilic, P. Christ, H. B. Li, E. Vorontsov, A. Ben-Cohen, G. Kassis, A. Szeskin, C. Jacobs, G. E. H. Mamani, G. Chartrand *et al.*, "The liver tumor segmentation benchmark (lits)," *Medical Image Analysis*, vol. 84, p. 102680, 2023. [5](#)

[38] *Proceedings of the Third International Symposium on Image Computing and Digital Medicine, ISICDM 2019, Xi'an, China, August 24–26, 2019*, 2019. [5](#)

[39] B. Landman, Z. Xu, J. Iglesias, M. Styner, T. Langerak, and A. Klein, "Medical image computing and computer-assisted intervention multi-atlas labeling beyond the cranial vault–workshop and challenge," in *Medical image computing and computer-assisted intervention*, vol. 5, 2015, p. 12. [5](#)

[40] J. Duchi, E. Hazan, and Y. Singer, "Adaptive subgradient methods for online learning and stochastic optimization," *Journal of machine learning research*, vol. 12, no. 7, 2011. [5](#)

[41] S. Gong, Y. Zhong, W. Ma, J. Li, Z. Wang, J. Zhang, P.-A. Heng, and Q. Dou, "3dsam-adapter: Holistic adaptation of sam from 2d to 3d for promptable medical image segmentation," *arXiv*, 2023. [5](#)

[42] W. Lei, X. Wei, X. Zhang, K. Li, and S. Zhang, "Medlsam: Localize and segment anything model for 3d medical images," *arXiv*, 2023. [5](#)

[43] J. Zhu, Y. Qi, and J. Wu, "Medical sam 2: Segment medical images as video via segment anything model 2," *arXiv*, 2024. [5](#), [6](#)

[44] Y. Xie, J. Zhang, C. Shen, and Y. Xia, "Cotr: Efficiently bridging cnn and transformer for 3d medical image segmentation," in *Medical image computing and computer-assisted intervention*, 2021, pp. 171–180. [6](#)

[45] N. Ravi, V. Gabeur, Y.-T. Hu, R. Hu, C. Ryali, T. Ma, H. Khedr, R. Rädle, C. Rolland, L. Gustafson *et al.*, "Sam 2: Segment anything in images and videos," *arXiv*, 2024. [6](#)

[46] L. R. Dice, "Measures of the amount of ecologic association between species," *Ecology*, vol. 26, no. 3, pp. 297–302, 1945. [5](#)